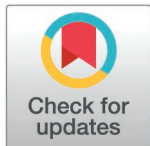RESEARCH ARTICLE

A novel *ex vivo* protocol that mimics length and excitation changes of human muscles during walking induces force losses in EDL but not in soleus of *mdx* mice

Xiao Hu[1], Allison N. McCrady[1], Katherine E. Bukovec[2], Claire Yuan[2], Emily Y. Miller[1], Rachel K. Bour[1], Anthony C. Bruce[1], Katherine B. Crump[1], Shayn M. Peirce[1], Robert W. Grange[2], Silvia S. Blemker[1,3,4]*

1 Department of Biomedical Engineering, University of Virginia, Charlottesville, Virginia, United States of America, **2** Department of Human Nutrition, Foods, and Exercise and Metabolism Core, Virginia Tech, Blacksburg, Virginia, United States of America, **3** Department of Orthopedic Surgery, University of Virginia, Charlottesville, Virginia, United States of America, **4** Department of Mechanical and Aerospace Engineering, University of Virginia, Charlottesville, Virginia, United States of America

☯ These authors contributed equally to this work.

* ssblemker@virginia.edu

Abstract

Although eccentric contraction protocols are widely used to study the pathophysiology and potential treatments for Duchenne muscular dystrophy (DMD), they do not reflect the stresses, strains, strain rates, and excitation profiles that DMD muscles experience during human daily functional tasks, like walking. This limitation of eccentric contractions may impede our understanding of disease progression in DMD and proper assessment of treatment efficacy. The goals of this study were to examine the extent of force loss induced by a gait cycling protocol we developed, and compare to that from a typical eccentric contraction protocol in soleus and extensor digitorum longus (EDL) muscles of *mdx* mice. To achieve this goal, *mdx* soleus and EDL muscles were subjected to eccentric contractions at three levels of strain (10%, 20% and 30% optimal length L_o) and up to 200 cycles of our gait cycling protocol that mimicked the length changes and excitation patterns of the corresponding muscles during human walking gait. Our results showed that EDL but not soleus muscles had significant losses in isometric tetanic forces after the cycling protocols. Compared to the eccentric contraction protocol, the decrements in contractile performance from the cycling protocol were similar to those from the eccentric contractions at 10% in soleus and 20% L_o in EDL. Together, these results indicated the gait cycling protocol is a valuable experimental approach to better understand disease progression and to screen and evaluate efficacy of novel therapeutics for DMD.

Introduction

Duchenne muscular dystrophy (DMD) is a severe monogenic disorder that leads to a non-functional dystrophin protein and subsequent loss of the dystrophin glycoprotein complex (DGC) from the sarcolemma of muscle cells [1,2]. The loss of the DGC results in progressive

muscle degeneration and weakness, which eventually causes cardiorespiratory failure and death in patients with DMD. Although substantial advances in therapeutic treatments have been made especially in recent years, there are still challenges to overcome before effective treatments may be developed [1,3,4]. One of the challenges is poor translation of promising outcomes from preclinical studies in animal models of DMD to treatment for patients with DMD. The ineffective translation may be largely due to physiological and biomechanical differences between the animal models and humans [5,6].

Eccentric contraction protocols [7–10] and treadmill exercises [11–13] to characterize dystrophic muscle in mouse models of DMD, such as the *mdx* mouse, have been widely used to study both the pathophysiology and potential treatments for DMD. *Ex vivo* eccentric contraction protocols lengthen muscles at a given rate while the muscles contract in response to a set electrical stimulation frequency to impose acute stresses. Although eccentric contraction protocols have helped advance the understanding and treatments of DMD, they do not reflect the stresses, strains, strain rates, and activation profiles that dystrophic muscles of human patients experience during daily repeated functional tasks, like walking. For example, in most eccentric contraction protocols, although the ranges of lengthening (usually under 30% of optimal length L_o) are generally within those encountered in walking [14], near maximal force production at a constant frequency of stimulation is typically applied, as muscles are lengthened at a fixed strain rate. In contrast, human muscles have time-varying force production and rate of length changes during walking, running, and moving up or down stairs; furthermore, force production only occasionally reaches a maximum [15,16]. During treadmill exercises, mice – as quadrupeds – employ more flexed postures during walking, which leads to substantially smaller strains in muscles compared to what human muscles may experience in walking [6]. These fundamental differences in force production and length change between *ex vivo* eccentric contraction protocols, treadmill exercises and human *in vivo* muscle function during daily tasks may impede our understanding of disease progression in DMD and limit proper assessment of treatment efficacy by relying primarily on *ex vivo* eccentric contraction protocols. Thus, it will be beneficial to replicate *in vivo* muscle activation (excitation), stresses and strains *ex vivo*.

Recently, we developed a novel *ex vivo* protocol to mimic muscle function in human daily tasks in dystrophic muscles in mouse models of DMD [17]. This protocol scales and adjusts the time-varying lengths and excitations experienced by muscles during human walking, so it can be mimicked in smaller isolated mouse muscles with equipment similar to that used for *ex vivo* eccentric contraction protocols. The time-varying muscle lengths and excitations are obtained from computer simulations of movement with detailed musculoskeletal models developed based on extensive imaging and dissection measurements [18,19]. In our proof-of-principle study [17], wild-type (WT) and *mdx* mice soleus muscles closely mimicked *in vivo* soleus muscle function during walking and well-tolerated 25 cycles of human walking gait, both of which indicated the feasibility of the protocol. However, it remains unclear how dystrophic muscles may respond to a larger number of repeated gait cycles *ex vivo*, as experienced during human daily walking, and how the responses of dystrophic muscles to this new protocol may differ from those of typical *ex vivo* eccentric contraction protocols.

The goal of this study was to test two hypotheses about the *ex vivo* cycling protocol. First, because the function of human lower limb muscles during walking may contribute to muscle degeneration in patients with DMD [6,20], we hypothesized that dystrophic soleus and extensor digitorum longus (EDL) muscles from *mdx* mice will demonstrate force loss when exposed to an *ex vivo* gait cycling protocol of several hundred gait cycles. Second, because our proof of concept study demonstrated limited damage in the *mdx* soleus subjected to 25 gait cycles [17], we hypothesized that the damage to *mdx* soleus and EDL muscles that resulted

from the *ex vivo* gait cycling protocol would be less severe than a typical *ex vivo* eccentric contraction protocol [9] for either soleus or EDL muscles. To assess these two hypotheses, up to 200 walking cycles were mimicked in soleus and EDL muscles using our *ex vivo* protocol of gait cycling [17] that scales the length changes of muscles based on architectural measurements and uses voltage modulation to excite mouse muscles in patterns close to human muscles in walking. Then, the muscle responses to this protocol were compared to those from an eccentric contraction protocol [9]. Our results highlight the differences between mouse and human muscle mechanics and the potential of the *ex vivo* gait cycling protocol as a valuable experimental approach to evaluate treatment efficacy and develop novel therapeutics for patients with DMD.

Methods

Animal and muscle preparation

All mouse protocols were approved by the Institutional Animal Care and Use Committee at Virginia Tech. Mice were fed standard chow, provided water ad libitum, and maintained on a 12-h light-dark cycle. Soleus and extensor digitorum longus (EDL) muscles from male C57BL/10ScSn-Dmd*mdx*/J mice at age 5–10 (7.7 ± 1.0) weeks (*mdx*; stock no. 001801, Jackson Laboratories), and C57BL/10ScSnJ mice at age 6–10 (8.0 ± 0.8) weeks (WT; stock No. 000476, Jackson Laboratories), were subjected to either an *ex vivo* eccentric contraction protocol [9] or an *ex vivo* gait cycling protocol that mimicked human walking gait [17]. The ages of the mice were chosen in our experiments because the literature showed that the degeneration and regeneration of hindlimb muscles of *mdx* mice are largely stabilized after ~ 6 weeks [21–23].

Mice were deeply anesthetized by an intraperitoneal injection of ketamine-xylazine (2 mg of ketamine-20 mg xylazine/100 g body mass), and once a deep plane of anesthesia was achieved, dissection began. The right and left soleus or EDL muscles were carefully dissected and 4-O suture tied to both proximal and distal myotendinous junctions [24]. The muscles were immersed in a jacketed water bath of physiological saline solution (PSS) maintained at 30°C [24]. Muscles from one side would undergo either eccentric contraction or gait cycling protocols (see the sections below), while those from the other side would serve as unstimulated controls that stayed in the experimental apparatus for the same duration. The unstimulated muscles provided information to check whether there were apparent damages to the muscle during the process of dissection and protocols. Mice were euthanized with an intracardiac injection of ketamine-xylazine, followed by cervical dislocation.

Pre-protocol contractions and measurements

Before the start of either the eccentric or the gait cycling protocols, the dissected soleus and EDL muscles were hung by clamping the distal suture at the bottom of the bath and the proximal suture tied to the arm of the dual-mode servomotor system (Aurora 300C-LR). Optimal muscle length (i.e., L_o) for soleus and EDL were determined as described [24]. Briefly, muscle resting tension was adjusted as an index of muscle length until the maximal twitch response was elicited [24]. A resting tension of 10 mN for both muscles yielded the maximum twitch response. All muscles were set to a resting tension of 10 mN followed by pre-contractions. Both the soleus and EDL muscles were stimulated to contract via platinum wire electrodes ~ 2 mm either side of the muscle. After 10 min of quiescence, 3 twitches (1 min apart) and 3 tetani at 150 Hz (1 min apart) were elicited at 30V. Resting tension was reset to 10 mN after each contraction. The muscle resting tension was stable for subsequent assays. Calipers were used to measure muscle length to the nearest 0.1 mm. After another 10 min of quiescence,

the pre-force frequency was conducted at L_o, with frequencies of stimulation varied from 1 Hz (twitch) to 180 Hz, with 1 min between each stimulation. In the pre-force frequency, the maximal isometric force was recorded.

Eccentric contraction protocol

An eccentric contraction protocol was followed as described [8,9] with some changes as noted below (Fig 1A; S1 Fig). Both WT and *mdx* soleus and EDL muscles were subjected to 5 eccentric contractions, with 4 min quiescence at L_o between each. For each eccentric contraction, both soleus and EDL muscles were stimulated at 80 Hz for a 500 ms isometric contraction, followed by a lengthening at 0.5 L_o/s for another 200 ms, 400 ms or 600 ms to yield a specific displacement of 10%, 20% or 30% L_o, respectively. Mice were divided into 3 different groups and muscles within each group were stretched to either 110%, 120% or 130% L_o to yield total strains of 10%, 20% or 30% L_o in eccentric contractions, respectively. At 5, 10, 15 and 30 min after the final stretch, tetanic (80 Hz) responses from the muscle were elicited to assess force recovery. After the final tetanic contraction, the muscles were incubated in a 0.2% procion orange/PSS solution (Reactive Orange 13, product number S477583-50MG, Sigma-Aldrich) for 60 min to assess membrane leakiness. Muscles were then washed two times, each time for 5 min in fresh PSS and lightly blotted; tendons were dissected free, and the mass to the nearest 0.1 mg was determined on an A-200D electronic analytical balance (Denver Instruments). Muscles were mounted for sectioning as described below.

Gait cycling protocol to mimic muscle function during human walking gait

The gait cycling protocol used to mimic muscle function during human walking gait was based on a dynamic musculoskeletal simulation of walking of a healthy human subject developed by John et al. [25] (https://simtk.org/projects/muscleprops) The technical details of this protocol were described in [17]. A brief description of the protocol is summarized below (Fig 1D).

The dynamic walking simulations reflected a healthy male (height: 1.83 m; weight: 65.9 kg) walking at 1.36 m/s on an instrumented treadmill (cadence: 109 steps/min; stride length: 1.45 m). A three-dimensional musculoskeletal model of human lower limbs [26,27] consisting of 12 body segments, 19 degrees of freedom, and 92 muscle-tendon units was used to develop this simulation in OpenSim [28]. Each muscle tendon unit was modeled as a Hill-type muscle model with muscle-specific architectural and geometric parameters to characterize its contraction dynamics and force-generating capacity [29]. From this simulation, time-varying values of excitation, fiber length, and force of soleus and EDL in one gait cycle were extracted to serve as inputs to the gait cycling protocol.

To mimic function of human muscles in mouse muscles with much smaller sizes, scaling based on muscle architectural parameters was applied. Specifically, the normalized lengths of muscles (either soleus or EDL) at each time instant t was calculated by:

$$\tilde{L}(t) = \frac{L^{human}(t)}{L_o^{human}} \tag{1}$$

where $L^{human}(t)$ is the simulation-predicted length of a human muscle fiber at time instant t during one gait cycle, and L_o^{human} (obtained from the lower limb musculoskeletal model) is the optimal fiber length of either soleus or EDL muscle. Then, the length changes with respect to the optimal fiber length in mouse muscle $\Delta L^{mouse}(t)$ were calculated as:

$$\Delta L^{mouse}(t) = \tilde{L}(t) * L_o^{mouse} - L_o^{mouse} \tag{2}$$
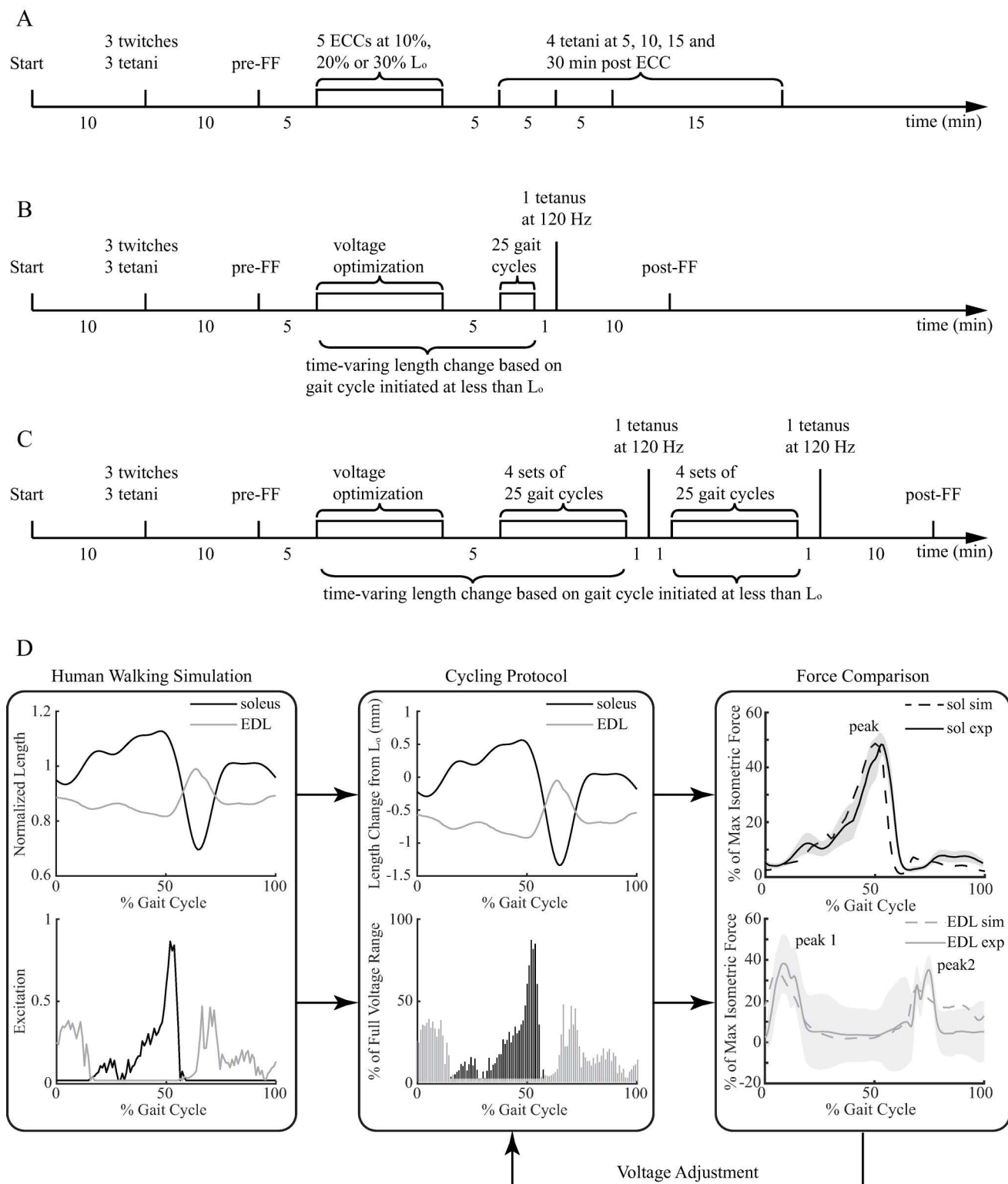
Fig 1. The timelines of the eccentric contraction (A), 25-cycle (B) and 200-cycle (C) gait cycling protocols. The protocol steps that were initiated at less than L_o were indicated in (B and C). The overview of the gait cycling protocol is shown in (D). sol: soleus; sim: simulation; exp: experiment.

Where L_o^{mouse} is the optimal fiber lengths of mouse soleus or EDL muscles [30]. The $\Delta L^{mouse}(t)$ would be used to vary mouse muscle length in the gait cycling protocol, which yielded length changes of about 40% and 20% L_o in soleus and EDL, respectively. Similarly, forces produced by human soleus or EDL muscles in walking gait were normalized by their corresponding maximum isometric forces in the lower limb model [26,27], and those by mouse soleus or EDL muscles were normalized by the corresponding measured maximum isometric forces in force-frequency stimulations. These normalized forces in human and mouse muscles were compared to adjust electrical stimulation intensity so that comparable forces were generated in mouse muscles in the gait cycling protocol.

To start the gait cycling protocol, muscles were first set and maintained at 10 mN resting tension (L_o), while they equilibrated in the bath. After equilibration, the following steps were performed: 1) pre-twitches and tetani (150 Hz), 2) pre-force frequency, 3) voltage optimization for gait cycling, 4) gait mimicking, and 5) post-force frequency (Fig 1B and C). Steps 1 and 2 were identical to those in the eccentric contraction protocol. In Step 3, to determine the voltage needed to produce the appropriate levels of force in mouse soleus and EDL muscles when mimicking walking gait, the initial voltage range was set to 0–20 V with a scale factor of 1. If the desired force levels were not achieved within this range, the voltage range was set to 0–80 V, and a scaling factor was used to adjust the force levels until the desired levels were reached (see *Additional excitation voltage modulation* in [17]). Once Step 3 was completed, and after 5 min of rest, the soleus or EDL muscle underwent either 25 or 200 consecutive cycles mimicking walking gait at a rate of 1 cycle/s. The 200 cycles were completed in multiple sets of 25 cycles with a 1-min rest in between. During the protocol, the rate of stimulation was synchronized with the rate of muscle length change at 222 Hz to achieve a smooth trajectory of length change. One minute following the completion of the 25th or 200th gait cycle, a 120-Hz tetanus was delivered at L_o. During the 200-cycle protocol an additional 120-Hz tetanus was elicited after the completion of the 100th cycle to check the muscle viability at the middle of the 200 cycles. Muscles then rested for 10 min at L_o, and the post-force frequency protocol was performed. The duration of the cycling protocols was within 1.5 hours. Note, all isometric and eccentric contractions were initiated with muscles at L_o (i.e., 10 mN) and all gait cycles were initiated with muscles at less than L_o to mimic the initial length of the human muscles (see Fig 1B and C) in a gait cycle.

Histological analyses

Soleus and EDL muscles were incubated in procion orange dye prior to sectioning to identify leaky fibers [8,9]. After completion of the 0.2% procion orange incubation and subsequent washes, muscles were embedded in 30% sucrose and optimal cutting temperature compound and flash frozen. The tissue blocks were then sectioned in a cryostat (NX50 Cryostar). To define the sarcolemmal membranes, the 10- um thick cryosections were fixed in 4% PFA, permeabilized with 0.3% triton, blocked with 10% donkey serum, incubated with α-2-laminin primary antibody (Sigma-Aldrich #L0663, clone 4H8-2) for one hour at 22°C, and incubated with donkey anti-rat secondary antibody conjugated to Alexa Fluor 488 fluorophore (Thermo Fisher Scientific, catalog # A-21208) for one hour at 22°C. Images were captured at 10X using a Nikon Eclipse C1 point scanning confocal microscope (Nikon Metrology Inc., Brighton, MI), independently fluorescing the red (procion orange) and then the green dyes (laminin).

Image tiles for each stain (procion orange and laminin) were manually stitched together for the individual images. The laminin image was then imported into FIJI [31] and the color threshold was set to show the most complete fiber borders. The image was then binarized and

any artifact fluorescence outside of the section was removed. The image was then transformed back to the green channel and exported to be overlaid with the procion orange image.

An automated image processing algorithm was developed in MATLAB (R2022b, Math-Works, Natick, MA) using user-defined segmentation parameters (i.e., adaptive thresholding sensitivity, number of outer layers removed, and gap removal to exclude any extraneous fibers segmented without boundaries present) to allow for visual optimization of the segmentations. The algorithm used contrast-limited adaptive histogram equalization to improve the contrast in the image [32]. The fiber image was then binarized using an adaptive threshold determined by the local mean intensity in the neighborhood surrounding the pixel [33]. This step was followed by enhancement methods to clear the image borders, and close pixel gaps in the fiber borders (green channel). The procion orange (red channel) was then binarized according to a global threshold [34] calibrated to the detectable amount of dye counted in 16 manual image segmentations by two trained analysts. The analysts were blind to the genotype and protocol group during segmentation. The fiber boundaries were then segmented using the binarized mask with 10 iterations of an active contouring algorithm [35] followed by a watershed transform [36] and then 15 iterations of the active contouring algorithm again. Watershed transform can lead to errors in segmentation due to noise within an image, therefore prior to transformation, the image was smoothed to suppress local minima. Multiple iterations of active contouring ensured smoothness of the fiber boundaries. Each fiber was then individually used as a mask on the binarized procion orange image, and the fiber was marked as positive for presence of dye if the area of procion orange fluorescence was greater than 50% of the fiber area. Following this analysis, the outer two layers of segmented fibers were removed due to the risk of damage during dissection, which may have resulted in high amounts of procion orange stain in those fibers. The percent of procion orange positive fibers (# positive fibers/# total fibers*100%) were exported with the final segmented image for further analysis. The difference in percent positive fibers from the automated segmentations versus the manual segmentations were: Analyst 1 average difference = 2.4%, median difference = 0.7%, maximum difference = 18.6% and Analyst 2: average difference = 1.1%, median difference = 0.8%, maximum difference = 5.6%. These values are similar to the differences between manual segmentation percent positive fibers between the two analysts (average difference = 3.1%, median difference = 1.4%, maximum difference = 16.9%).

Data processing and statistics

To compare the force losses and recoveries during the eccentric contraction protocols, the forces from each of five eccentric contractions and during recovery for each muscle were normalized to the forces from the first eccentric contraction for that muscle. When comparing force losses and recoveries during the gait cycling protocols, the dynamic peak forces from each gait cycle (Fig 1D) and the isometric tetani during recovery for each muscle were recorded and normalized to maximum isometric forces from that muscle's pre-force frequency profile. Means and standard errors of the mean were then determined for either the groups of muscles subjected to the eccentric protocol or to the gait cycling protocols. The comparisons between the eccentric contraction protocols and the gait cycling protocols were made using the force responses measured at 80 Hz 10 minutes after the eccentric contractions were complete, and from the 80 Hz response obtained during the post-force-frequency 10 minutes after the gait cycling protocol was complete. The force responses 10 minutes after the completion of both protocols were selected for the comparison to minimize the potential effect of fatigue. All force responses at 80 Hz were normalized to the forces at 80Hz from the pre-force-frequency profile for either of the two protocols, which indicates the level of force losses after the protocols (i.e., normalized force smaller than 1 indicates a force loss) as a

measure of damage to the contractile function of muscle [9,10,37]. All muscles for these comparisons had force responses elicited at L_o.

Linear mixed-effects (LME) models [38] with genotypes and number of eccentric contractions (for the eccentric contraction protocol) or number of cycles (for the gait cycling protocol) as fixed effects and mice as a random effect were used to examine the effects of genotypes and eccentric contractions or gait cycles on the force losses in the respective protocols. Similar LME models with genotypes and time of the force measurements as fixed effects and mice as a random effect were used to examine the effects of genotypes and force recovery after the eccentric and gait cycling protocols. When comparing the cycling protocols and eccentric contraction protocols, LME models were used to examine the effect of protocols (as a fixed effect) on the recovery forces after the two protocols. LME models were used to account for the repeated measures (e.g., multiple eccentric contractions or gait cycles) from the same sample during protocols. The sequential Bonferroni correction (Holm-Bonferroni method) was used to control all the pairwise comparisons from each of the LME models [39]. These statistical analyses were conducted in Matlab (R2022b, Mathworks, Natick, MA, United States) with the significance level set at $p < 0.05$.

The percent of dye-positive fibers of each sample were used for final comparative analysis. Statistical outliers for each group were removed using the Dixon method [40]. For each variable, a two-way ANOVA (genotype, injury protocol) with a Tukey's post hoc test was used. R Statistical Programming Software (v4.2.2, R Core Team 2021) and a significance level at $p < 0.05$ were employed.
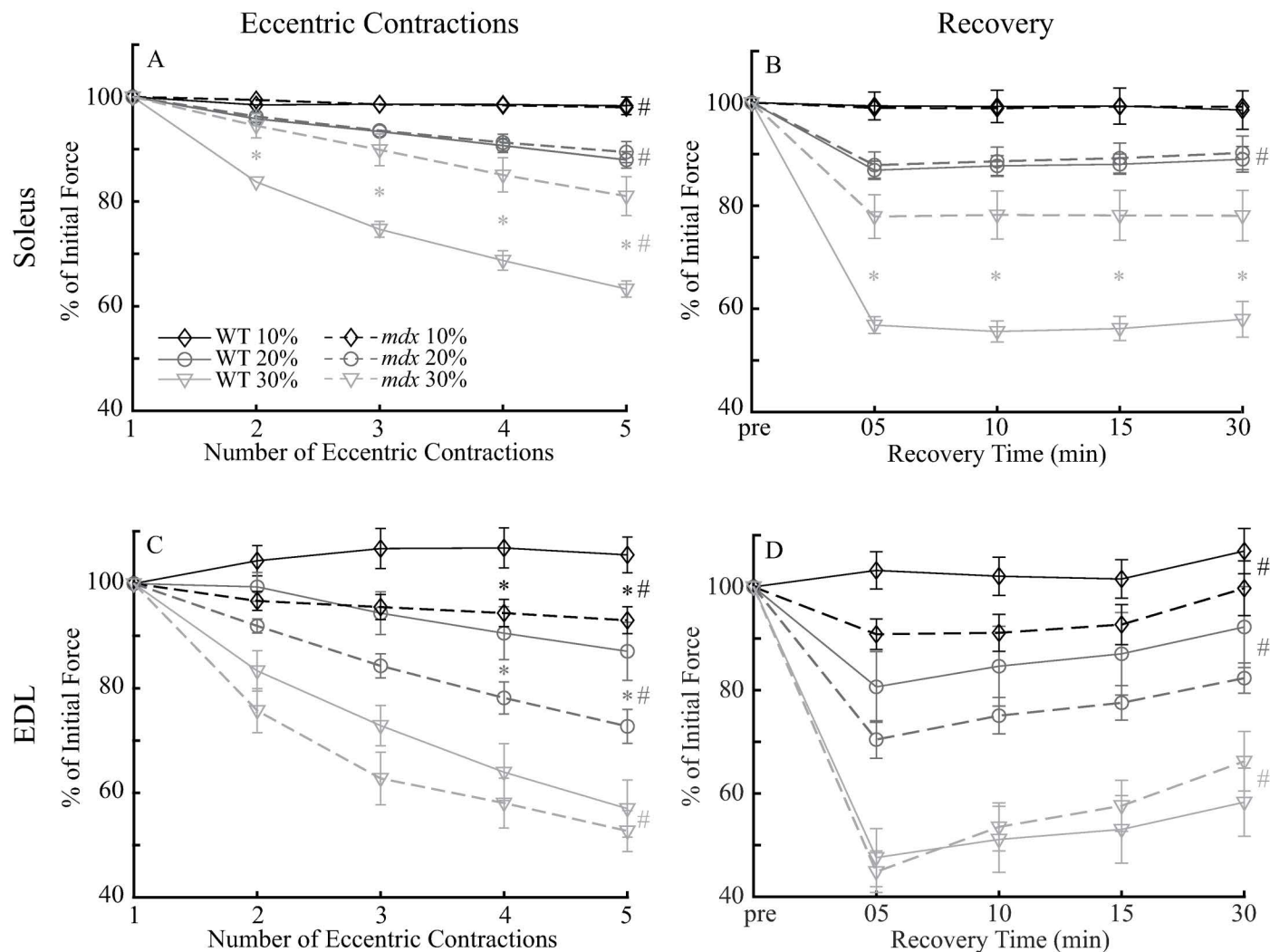
Results

Eccentric contraction protocol

As previously reported in the literature, *mdx* soleus muscle tolerated eccentric contractions similar to WT soleus muscle, while *mdx* EDL muscle generally had greater force losses due to the eccentric contractions compared to WT EDL muscle. After five eccentric contractions at 10% and 20% L_o, soleus muscles in both genotypes only lost about 2% and 10% of the initial force, respectively (Fig 2 A). There were no differences in force responses between the WT and *mdx* soleus muscles (all $p > 0.3$) at either 10% or 20% L_o. The eccentric contractions at 30% of L_o led to 38% and 19% losses of force in WT and *mdx* soleus, respectively, with *mdx* soleus showing significantly less force loss from contractions 2–5 (all $p < 0.01$). In contrast to soleus, *mdx* EDL muscle showed significantly greater force losses from eccentric contractions 3–5 at 10% L_o (all $p < 0.05$) and from eccentric contractions 4 and 5 at 20% L_o (both $p < 0.05$; Fig 2C). During eccentric contractions at 30% L_o, EDL muscles from both genotypes lost comparable amounts of force (all $p > 0.3$) that reached over 40% after five eccentric contractions.

After the eccentric contractions were complete, the soleus muscle generally did not show much recovery of force loss, whereas the EDL muscle showed significant recovery within 30 minutes. After eccentric contractions at 10% and 30% L_o, the WT and *mdx* soleus muscles did not show recovery of isometric tetanic force following ECC within 30 minutes of the final eccentric contraction (e.g., from 05–30 min, both $p > 0.7$; Fig 2B). After eccentric contraction at 20% L_o, although the recovery was statistically significant ($p < 0.01$), the actual recovery was only about 2%. There was no genotype difference in recovery of soleus at 10% and 20% L_o (both $p > 0.7$). However, after eccentric contractions at 30% L_o, tetanic forces (at 80 Hz) of WT soleus were lower than those of *mdx* soleus at all four recovery time points (all $p < 0.001$). In contrast to the soleus muscle, the WT and *mdx* EDL muscles showed significant recovery at all three stretch magnitudes of eccentric contractions (all $p < 0.01$; Fig 2D). In addition, there was no difference in recovery between the two genotypes (all $p > 0.05$).

Fig 2. The force reduction resulted from a series of five eccentric contractions at 10%, 20% and 30% L$_o$ from WT and *mdx* soleus (A) and EDL (C) and recovery of isometric tetanic force following eccentric contraction protocol in WT and *mdx* soleus (B) and EDL (D) muscles. All forces were normalized to the isometric force before the 1st eccentric contraction. Data shown are mean ± SEM. The SEMs smaller than the symbols are not shown. * differences between WT and *mdx*. # significant main effects of number of eccentric contractions (A and C) and recovery time (B and D) in both WT and *mdx* mice. All comparisons $p <$ 0.05. pre: the isometric force before the 1st eccentric contraction. Soleus: 10% L$_o$, n = 10 for WT and *mdx*; 20% L$_o$, n = 10 for WT and *mdx*; 30% L$_o$, n = 8 for WT and 9 for *mdx*. EDL: 10% L$_o$, n = 10 for WT and 8 for *mdx*; 20% L$_o$, n = 10 for WT and *mdx*; 30% L$_o$, n = 15 for WT and 14 for *mdx*.

https://doi.org/10.1371/journal.pone.0320901.g002

Gait cycling protocol

Soleus and the EDL muscles had significant force losses after undergoing gait cycling protocols that mimicked the length changes and activation profiles of these two muscles in human walking. In the 25-cycle protocol, peak forces of both the soleus and EDL muscles were reduced significantly at the 25th cycle compared to the 1st cycle (Fig 3A, 3C and 3E; soleus: $p <$ 0.001; EDL: $p <$ 0.001 for peak 1 and peak 2). There was no difference in force loss (difference in peak force between the 1st and 25th cycles) between the two genotypes for soleus ($p = 0.21$) or for EDL (peak1: $p = 0.72$; peak 2: $p = 0.55$). Similarly, in the 200-cycle protocol, peak forces of both the WT and *mdx* soleus and EDL muscles were reduced due to the repeated gait cycles (Fig 3B, 3D and 3F; soleus: $p <$ 0.001; EDL $p <$ 0.001 for peak 1 and peak 2). There was no
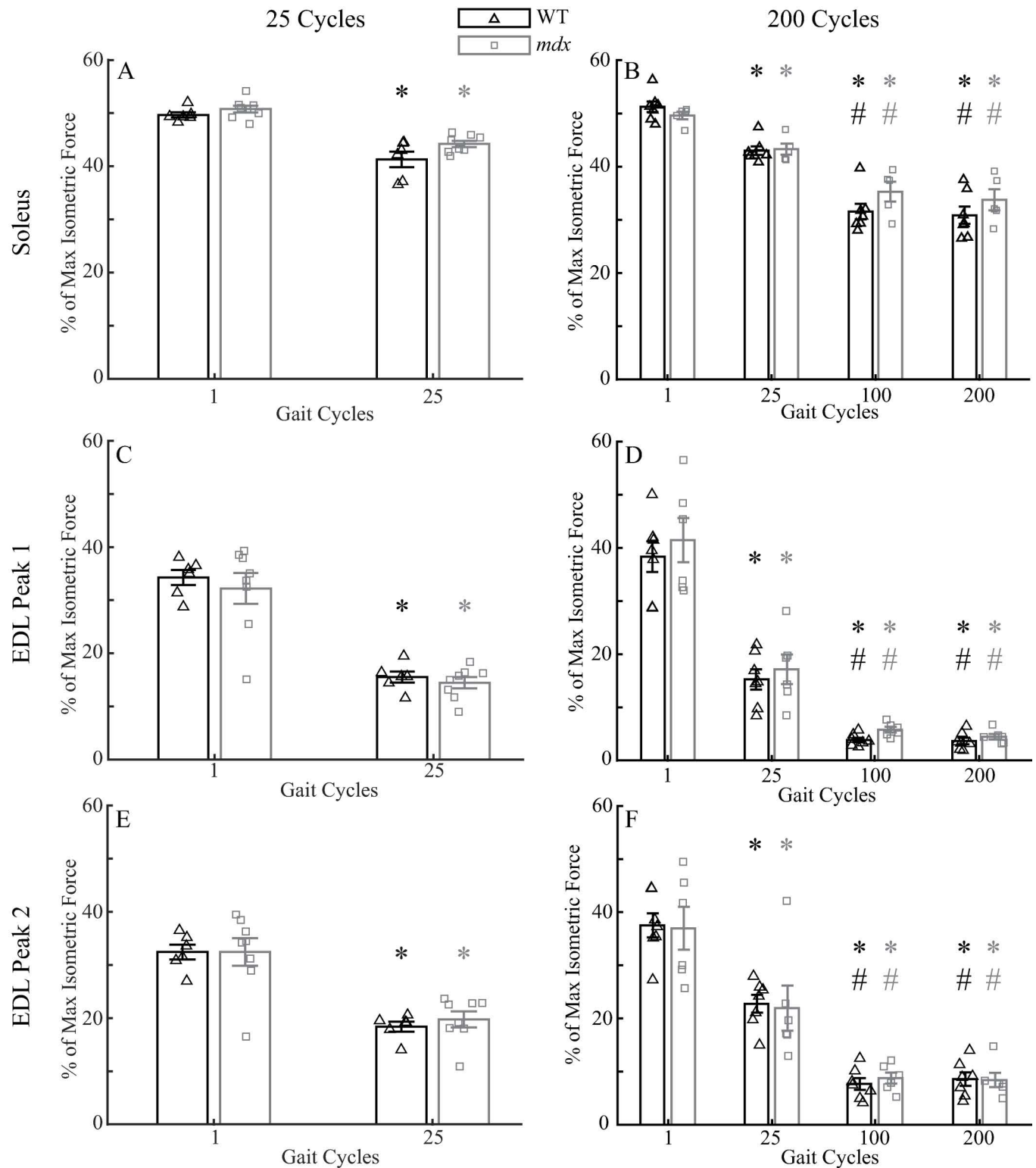
Fig 3. Comparisons of forces in soleus muscles in the 25-cycle (A) and 200-cycle (B) protocols, and those in EDL muscles in the 25-cycle (C and E for Peak 1 and 2, respectively) and 200-cycle (D and F for Peak 1 and 2, respectively) protocols. All forces were normalized to the maximum isometric tetanic force measured during the pre-force frequencies. Data shown are mean ± SEM. * differences from 1st cycle at $p < 0.01$; # differences from 25th cycle at $p < 0.01$. Soleus: 25-cycle, n = 6 for WT and 8 for *mdx*; 200-cycle, n = 7 for WT and 5 for *mdx*. EDL: 25-cycle, n = 6 for WT and 8 for *mdx*; 200-cycle, n = 7 for WT and 6 for *mdx*.

difference in force loss between the two genotypes for soleus (25th cycle: p = 0.31; 100th cycle: p = 0.10; 200th cycle: p = 0.18) or for EDL (25th cycle: p = 0.73 for peak 1 and p = 0.93 for peak 2; 100th cycle: p = 0.81 for peak 1 and p = 0.71 for peak 2; 200th cycle: p = 0.64 for peak 1 and p = 0.94 for peak 2). There was a greater force loss at the 200th cycle than at the 25th cycle (soleus: WT and p < 0.01; EDL: both WT and *mdx* p < 0.01 for peak 1 and peak 2). The force loss largely plateaued after the 100th cycle in both muscles. There was no difference in peak forces between the 100th and 200th cycles (soleus: WT p = 0.64, *mdx* p = 0.38; EDL: WT p = 0.94, *mdx* p = 0.62 for peak 1 and WT p = 0.73, *mdx* p = 0.90 for peak 2).

Although the peak forces of both soleus and EDL were reduced during the gait cycling protocol, only the isometric tetanic forces (at 120Hz) of EDL were reduced after compared to before the gait cycling protocol, and this reduction of tetanic force did not recover 10 minutes after the protocol. Soleus muscles had increased maximum isometric forces 1 minute after the 25-cycle protocol compared to that before the protocol (both genotypes p < 0.001; Fig 4A). This enhanced isometric force decreased 10 minutes after the protocol in WT soleus (p < 0.01), but not in *mdx* (p = 0.09). However, WT soleus still demonstrated increased isometric force 10 minutes after the protocol than before the protocol (p < 0.01), while the isometric force of *mdx* soleus 10 minutes after was comparable to that before the protocol (p = 0.09). In contrast, EDL muscle had reduced maximum isometric forces 1 minute (both genotypes p < 0.01) and 10 minutes (both genotypes p < 0.01) after the 25-cycle protocol compared to those before the protocol (Fig 4C). Resting for 10 minutes did not significantly alter the levels of the maximum isometric forces in the EDL muscle (both genotypes p > 0.8). There were no genotype differences in soleus and EDL at all tested times (p > 0.1 for soleus and EDL) with the only exception in soleus at 1 minute after the protocol (p < 0.05).

The maximum isometric forces at 120 Hz in soleus and EDL muscles after the 200-cycle protocol followed similar patterns. One minute after the 200-cycle protocol, *mdx* soleus had an increased isometric force compared to that before the protocol (p < 0.05; Fig 4B). This increased force generating ability also existed in the middle (e.g., inter, at 120Hz) of the protocol (p < 0.05), but diminished 10 minutes after the protocol (p = 1). The WT soleus did not show an increased isometric force generating ability in the middle (e.g., inter, p = 0.49), 1 minute after (p = 0.99), and 10 minutes after (p = 1) the 200-cycle protocol. The EDL muscle had reduced maximum isometric forces in the middle of (e.g., inter, WT p < 0.001; *mdx* p = 0.15), 1 minute after (both genotypes p < 0.001), and 10 minutes after (both genotypes p < 0.001) the 200-cycle protocol compared to that before the protocol (Fig 4D). Resting 10 minutes did not have any effects on the isometric forces of EDL muscle (WT p = 0.95; *mdx* p = 0.48). There were no genotype differences for soleus or EDL at all tested times (p > 0.1 for soleus and EDL) with the only exception being soleus at 1 minute after the protocol (p < 0.05).

Dye uptake

The gait cycling protocols did not alter the amount of dye uptake in WT and *mdx* soleus and EDL muscles. After the cycling protocols, the soleus muscles showed no differences among the groups (no injury vs. 25 cycles vs. 200 cycles; p = 0.94) and between genotypes (WT vs. *mdx*; p = 0.31; Fig 5A). Although the EDL muscles showed significant main effects among groups (no injury vs. 25 cycles vs. 200 cycles; p = 0.04) and between genotypes (WT vs. mdx; p < 0.01) after the cycling protocols (Fig 5B), the 25-cycle protocol did not increase the dye uptake in WT (p = 0.99) and *mdx* EDL (p = 0.17) muscles compared to the no-injury group. Similarly, the 200-cycle protocol did not increase the dye uptake in WT (p = 0.99) and *mdx* EDL (p = 0.30) muscles compared to the no-injury group.
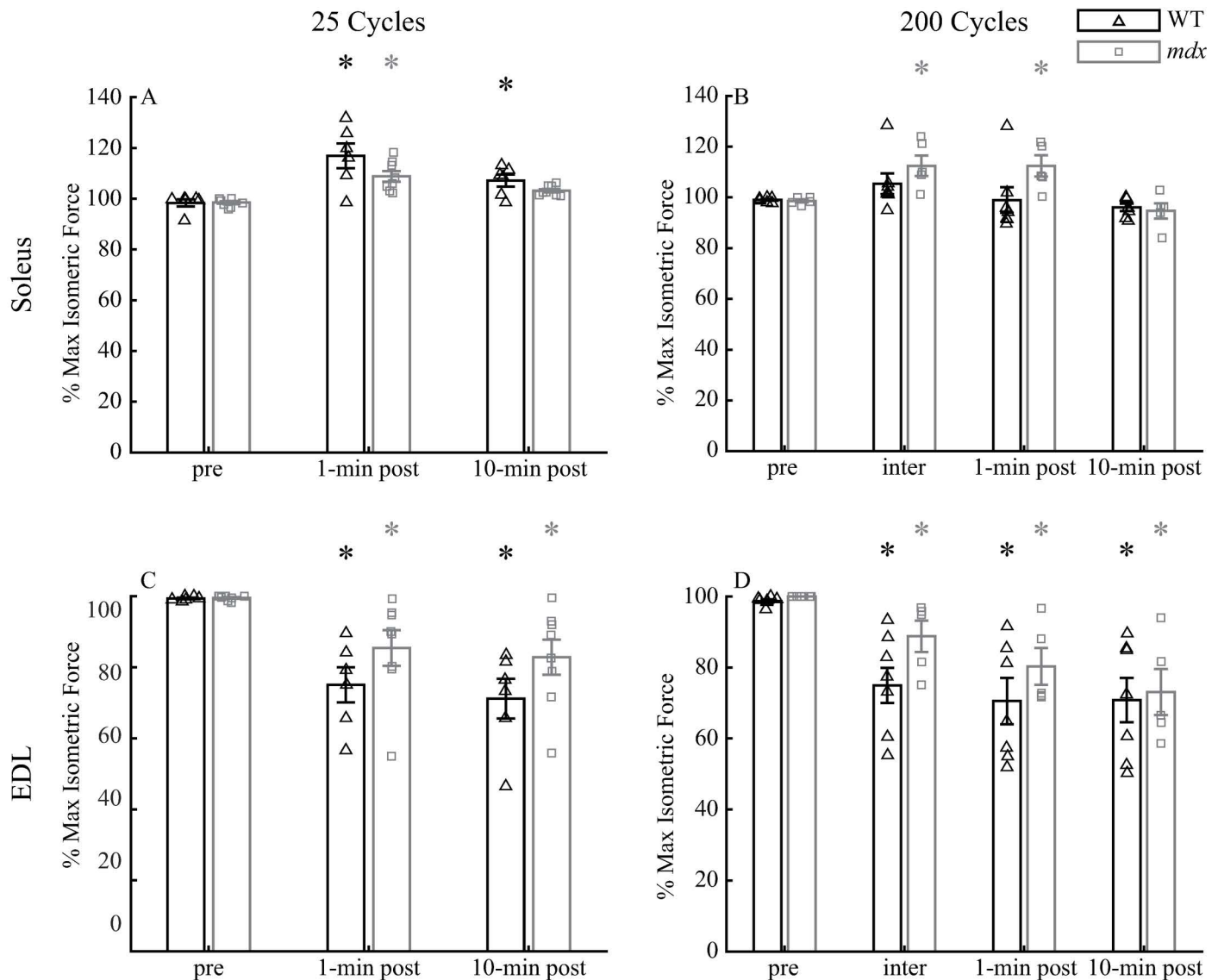
Fig 4. Comparisons of isometric tetanic forces at 120 Hz in soleus muscles in the 25-cycle (A) and 200-cycle (B) protocols, and those in EDL muscles in the 25-cycle (C) and 200-cycle (D) protocols. All forces were normalized to the maximum isometric tetanic force measured during the pre-force frequencies. Data shown are mean ± SEM. * differences from pre at $p < 0.05$. pre: 120Hz tetanus during force-frequency before the protocol; 1-min post: a 120 Hz tetanus 1 minute after the protocol; 10-min post: a 120Hz tetanus during force-frequency 10 minutes after the protocol; inter: a 120 Hz tetanus after the 100th cycle in 200-cycle protocol. Soleus: 25-cycle, n = 6 for WT and 8 for *mdx*; 200-cycle, n = 7 for WT and 5 *mdx*. EDL: 25-cycle, n = 6 for WT and 8 for *mdx*; 200-cycle, n = 7 for WT and 5 for *mdx*.

https://doi.org/10.1371/journal.pone.0320901.g004

Comparison between eccentric and cycling protocols

When comparing the tetanic forces (at 80Hz) 10-minutes after the conclusion of the protocols normalized to values before the protocols, soleus and EDL muscles that underwent the gait cycling protocols largely showed higher or comparable forces compared to those that underwent the eccentric protocols. After the 25-cycle protocol, the WT and *mdx* soleus muscles showed higher normalized forces than those after eccentric contraction protocols (WT: *p* < 0.01 for 25 cycles vs. eccentric contractions at 10%, 20%, and 30% L$_o$; *mdx*: *p* < 0.01 for 25 cycles vs. eccentric contractions at 20% and 30% L$_o$; Fig 6A). The only exception was the
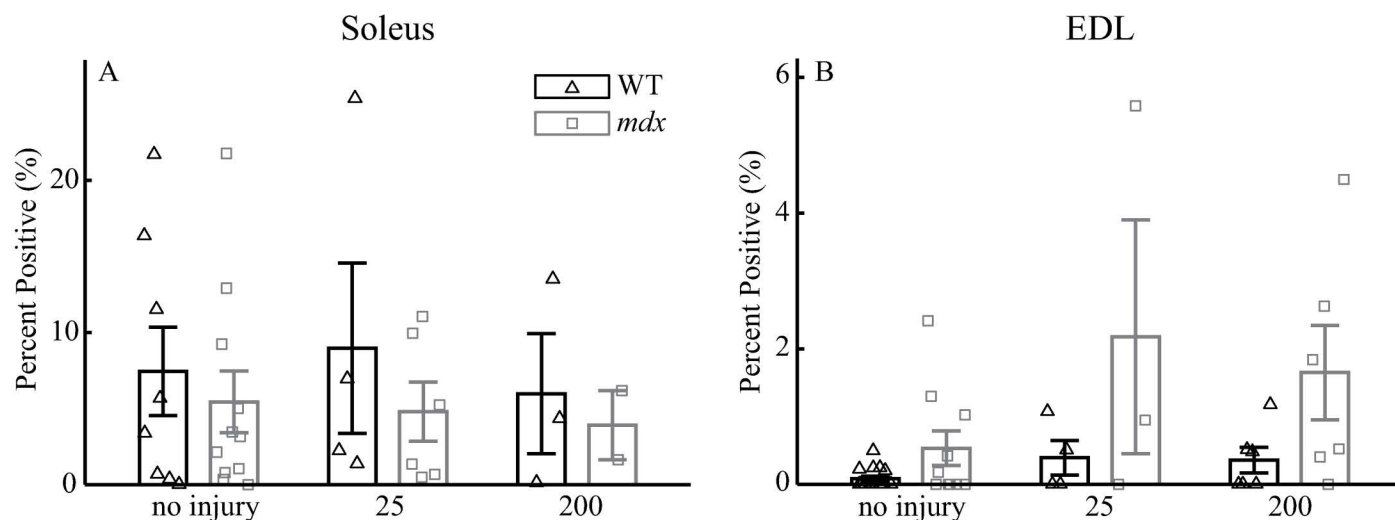
Fig 5. Comparisons of dye uptake after 25-cycle and 200-cycle protocols for Soleus (A) and EDL (B). Data shown are mean ± SEM. EDL muscles showed significant main effects among groups (no injury vs. 25 cycles vs. 200 cycles; $p = 0.04$) and between genotypes (WT vs. mdx; $p < 0.01$) after the cycling protocols. Soleus: no injury, n = 8 for WT and 11 for *mdx*; 25-cycle, n = 4 for WT and 6 for *mdx*; 200-cycle, n = 3 for WT and 2 for *mdx*. EDL: no injury, n = 16 for WT and 10 for *mdx*; 25-cycle, n = 4 for WT and 3 for *mdx*; 200-cycle, n = 6 for WT and 6 for *mdx*.
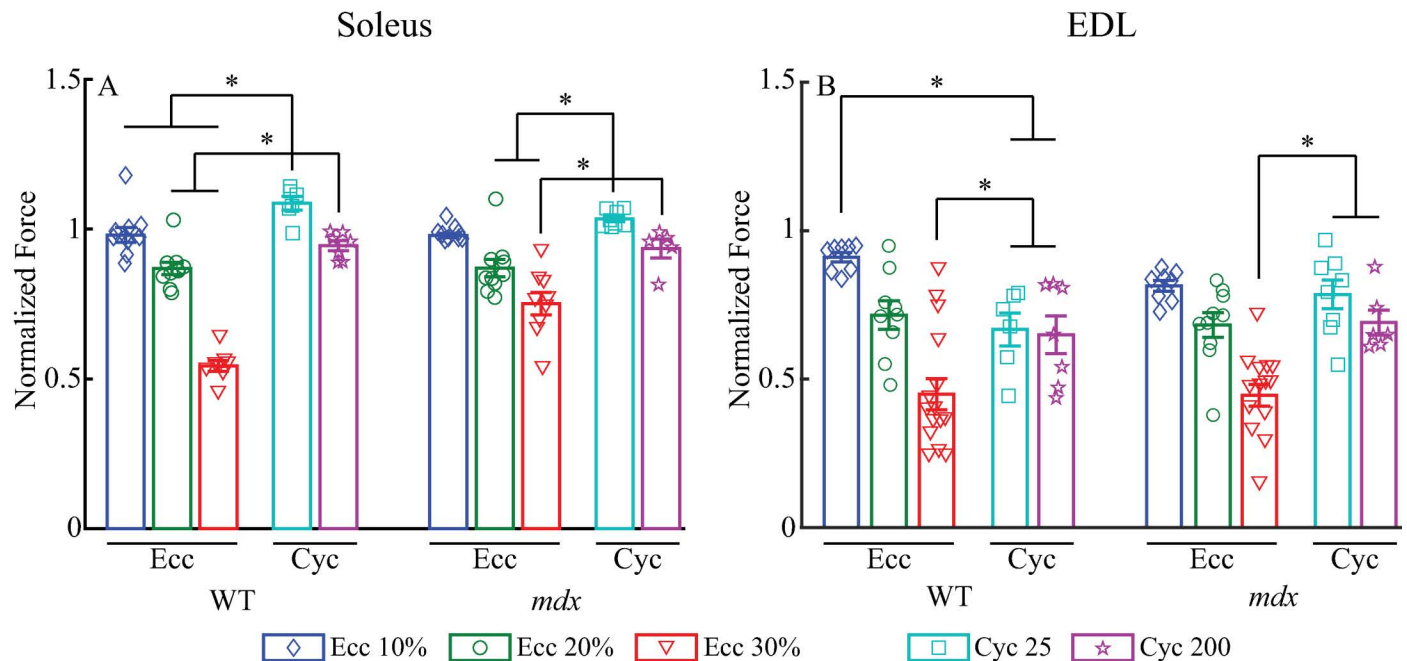
mdx soleus after the eccentric contraction at 10% L_o, which had comparable forces to those after 25-cycle protocol ($p = 0.36$). For EDL muscles, normalized forces 10 minutes after the 25-cycle were comparable to those after eccentric contraction protocol at 10% L_o for *mdx* ($p > 0.05$) and at 20% L_o for both WT ($p > 0.3$) and *mdx* ($p > 0.3$; Fig 6B). Normalized forces were higher than those at 30% L_o ($p < 0.05$ for WT and *mdx*). Only normalized forces of WT EDL after the 25-cycle were lower than after the eccentric contraction at 10% ($p < 0.05$). After the 200-cycle protocol, the WT soleus muscles had higher forces than those after eccentric contraction at 20% L_o ($p < 0.05$) and 30% L_o ($p < 0.01$), but comparable forces to those after eccentric contraction at 10% L_o ($p > 0.3$; Fig 6A). Similarly, the *mdx* soleus muscles had higher forces than those after eccentric contraction at 30% L_o ($p < 0.01$), but comparable forces to those after eccentric contraction at 10% L_o ($p > 0.3$) and 20% L_o ($p > 0.1$). For EDL muscles after the 200-cycle protocol, normalized forces were comparable to those after eccentric contraction protocol at 10% L_o for *mdx* ($p > 0.2$) and at 20% L_o for both WT ($p > 0.8$) and *mdx* ($p > 0.8$; Fig 6B). Normalized forces were higher than those at 30% L_o ($p < 0.05$ for WT and *mdx*). Only normalized forces of WT EDL after the 200-cycle were lower than those after the eccentric contraction at 10% ($p < 0.05$).

Discussion

Two hypotheses regarding the *ex vivo* cycling protocol were examined in this study: 1) dystrophic soleus and EDL muscles from *mdx* mice would demonstrate damage when exposed to repeated changes in length, force and excitation that mimic those that corresponding human muscles experience in a cyclic human walking gait pattern; and 2) the damage to dystrophic soleus and EDL muscles revealed by the *ex vivo* gait cycling protocol would be less severe than a typical *ex vivo* eccentric contraction protocol [9]. Our results showed that only EDL muscles had significant losses in the isometric tetanic forces after the cycling protocols, while soleus muscles did not. However, both soleus and EDL muscles had significantly reduced peak forces in the last gait cycle (either 25th or 200th) compared to the 1st cycle during the gait cycling protocols. Our results also showed that, after the gait cycling protocols, soleus and EDL muscles

Fig 6. Comparisons between the cycling and eccentric contraction protocols in soleus (A) and EDL (B) muscles. All forces were from 80Hz tetani 10-minute after the protocols and normalized to forces of the 80 Hz tetani before the corresponding protocols. Data shown are mean ± SEM. * differences between compared protocols ($p < 0.05$).

https://doi.org/10.1371/journal.pone.0320901.g006

produced higher or similar forces compared to those after the eccentric protocols, which suggested less severe or similar effects on contractile performance.

WT and *mdx* soleus and EDL muscles subjected to repeated gait cycles that mimicked the stresses, strains, and excitation patterns of these muscles during human walking gait revealed force losses in the EDL but not in the soleus. Although the dynamic peak forces during the gait cycling protocols were reduced in both soleus and EDL muscles (Fig 3), the isometric tetanic forces at 120Hz 1-min and 10-min post the cycling protocol, which reflect muscle force-generating capacity [9], were only reduced in EDL, but not in soleus (Fig 4). In fact, soleus muscles demonstrated increased tetanic force after the gait cycling protocols (see more discussion below). These outcomes suggested that it was likely that the decreased dynamic peak forces in EDL muscles resulted from a combination of fatigue and reduced force generating capacity, whereas fatigue may be the main cause for the decreases in the dynamic peak forces of soleus muscle during cycling protocols [41]. The different sensitivities of soleus and EDL to the cycling protocols are similar to those in eccentric contraction protocols, in which eccentric contractions at 10% and 20% L_o only induce minimal, comparable force losses in WT and *mdx* soleus muscles [42].The damage to the EDL but not to the soleus muscles after the cycling and eccentric contraction protocols may be due to more slow fiber, utrophin and cytoplasmic actin content in soleus compared to the EDL muscle [10,43]. In addition, while pennation angle is similar between the two muscles [44], more complex features of muscles' architectures, such as fiber curvature and aponeurosis morphology may also play a role [45,46]. Our results together with previous studies [10,42] showing insensitivity of soleus to eccentric contraction protocols indicate that soleus muscle may not be a good candidate for pre-clinical studies that intend to understand disease progression and to evaluate the efficacy of treatments for DMD.

When comparing the gait cycling protocol to the eccentric contraction protocol [9], it appeared that the decrement in contractile performance, as indicated by force losses, is similar to that from the 10% and 20% L_o eccentric contraction protocols, but smaller than the 30% L_o eccentric contraction protocol (Fig 6). The eccentric contraction at 30% L_o had a large strain magnitude that can elicit substantial force losses both in soleus and EDL muscles [43]. Although soleus and EDL muscles in the gait cycling protocol had lengthening strains up to 30% L_o, they were under submaximal activation during the majority of a gait cycle [15]. As activation level strongly affects the magnitude of force losses after eccentric contractions, in the gait cycling protocols the submaximal activation yielded less than maximum isometric forces, which potentially resulted in smaller force losses or contractile impairment [47,48]. Other than the soleus muscles in the 25-cycle protocol that showed some increased forces, the force losses in soleus from the cycling protocol were close to the negligeable losses elicited from eccentric contractions at 10% L_o in soleus. For EDL muscles, the force loss from the cycling protocol was close to that elicited from eccentric contractions at 20% L_o, which may suggest that the eccentric contractions at 20% L_o with a strain rate of 50% L_o/s and 5 repetitions may reflect the effects of human walking gait experienced by EDL muscles. Surprisingly, our results showed that eccentric contractions at 30% L_o induced more force losses in WT than in *mdx* soleus muscles (Fig 2). There were only a limited number of studies that examined the force losses of soleus from *mdx* mice after eccentric contractions, which typically lengthened muscle up to 20% L_o and showed no differences between the WT and *mdx* [10,42,49,50], consistent to our results at 10% and 20% L_o. The greater force losses in WT than in *mdx* soleus muscles at 30% L_o may be due to the a greater peak active force produced by the WT soleus during eccentric contractions at this magnitude, which led to the disruptions of sarcomere and/or the excitation-contraction coupling process that caused the greater force loss [51,52].

There were no differences between the genotypes in the responses of soleus and EDL muscles to the gait cycling protocols (Fig 3), which may be due to the differences in histopathology between hindlimb muscles in *mdx* mice and lower limb muscles in patients with DMD. Given that the hindlimb muscles in *mdx* mice are much less affected than human DMD lower limb muscles [53], it is plausible that when physiologically relevant loadings that mimicked human walking were applied, no significant differences were shown between WT and *mdx* mice. Mimicking stresses and strains in dystrophic muscles from mouse models that better recapitulate the histopathology of DMD, such as the D2.*mdx* [54], may elicit divergent responses from WT and dystrophic muscles. In addition, the cycling protocol can be slightly modified to mimic the walking pattern of boys with DMD, which have demonstrated some kinematic and kinetic differences from healthy boys and adult males [55–58]. Or, the cycling protocol can mimic daily activities that demand more stressful eccentric contractions from lower limb muscles, such as walking downhill or descending stairs, than level ground walking [59,60], to elicit different responses from WT and *mdx* muscles. Although traditional eccentric contraction protocols elicit more force losses in fast-twitch muscles between WT and *mdx* mice [37], the more physiologically relevant cycling protocol may improve the transferability of preclinical findings in mouse models of DMD to patients.

The increased tetanic force in the soleus muscle after the gait cycling protocol was unexpected. However, there are several possible mechanisms that may have led to this observation (Fig 4). One possible mechanism may be the residual force enhancement potentially induced by the elasticity of titin [61]. Residual force enhancement contributes to increased isometric force after cycles of shortening and lengthening [62,63] and the increased isometric force can be greater than the maximum isometric force at L_o.[64]. So, it is plausible that after repeated shortening and lengthening in the gait cycling protocol, soleus muscles in our study

showed increased isometric force over the force at L_o before the protocol due to residual force enhancement. However, it has been reported that the enhanced force disappears if electrical stimulation to the muscle is interrupted [65]. Because in our experiment the soleus force was measured after a 1-minute rest following the cycling protocol, residual force enhancement may not be responsible. Another possible mechanism is force potentiation related to phosphorylation of the myosin regulatory light chains due to prior activation that increased the Ca^{2+} sensitivity of contraction [66]. However, force potentiation has been mostly observed in muscles dominated with predominant fast-twitch fibers, rather than those with mostly slow-twitch fibers, like soleus [67]. In addition, the fast-twitch EDL muscle did not show signs of force potentiation after the gait cycling protocol. Thus, it seems unlikely that the force potentiation increased soleus force observed after the gait cycling protocols.

It was surprising that, even though gait cycling protocols lead to loss in force production, we did not observe significant differences in procion orange dye uptake (Fig 5). Our results indicated no difference between non-injured and injured muscles across genotype. While previous work has reported differences in sarcolemmal leakiness measured via procion orange dye uptake in these limb muscles between *mdx* and WT mice after eccentric contractions, our results from muscles subjected to the gait cycling indicated *mdx* samples generally had a large dye uptake that was higher in non-injured samples [8,68]. Future work is necessary to investigate alternative markers of sarcolemmal damage such as Evan's Blue Dye or H&E staining [69].

Current skeletal muscle immunohistochemistry segmentation methods are limited and may be highly variable due to a variety of factors. Detailed skeletal muscle immunohistochemistry segmentation is often manual, observer dependent, and time-consuming [70]. This analysis could vary based on the observer's visual acuity, as well as dexterity to quantify the fiber morphology such as cross-sectional area or shape through manual segmentation [71,72]. Additionally, manual analysis can introduce user bias when doing a comparative study as the observer may not be blinded to the condition. The current literature does not provide detailed methods of quantification such as what intensity level or the amount of fiber cross-section positively stained is determined as a positive fiber, allowing for variability in inter-observer counts and non-standard implementation [9,73,74]. Recent advances in image segmentation techniques have resulted in several opensource platforms; however, these platforms still require a large degree of oversight which is not easily viable in large experimental studies [75,76]. Due to these limitations, we designed and employed a segmentation algorithm to standardize the quantification of dye across samples. Our algorithm was compared to the gold standard manual quantification from two skilled analysts for randomly selected samples with great agreement (within 3%).

The gait cycling protocol does have some limitations. First, when mimicking walking gait, to ensure that the forces in mouse soleus and EDL muscles were comparable to the corresponding human muscles, voltage modulation was needed for each individual muscle. With some practice, this voltage modulation could be completed within several gait cycles [17]. Although this extra step may have increased the time duration of the cycling protocol, the viability of the muscles was maintained, because the isometric tetanic forces did not differ within, 1-min after, or 10-min after the 200-cycle protocol (Fig 4). Second, fatigue may contribute to the decrease of dynamic peak forces in the cycling protocol. Thus, isometric tetani and appropriate rests after the gait mimicking cycles are needed to probe the actual force loss due to the damage to the muscle contractile properties by the protocol.

This study explored the use of the gait cycling protocol to mimic the stresses, strains and excitation patterns of human soleus and EDL muscles during level ground walking in the corresponding muscles in WT and *mdx* mice. By closely replicating *in vivo* human muscle

functions in activities, this protocol reduces the biomechanical differences in muscle function between humans and mice that may hinder the application of mouse models in pre-clinical studies [6]. The damaging effects to the contractile performance from the cycling protocol were similar to those from the eccentric contractions at 20% L_o. This outcome suggests potential of the cycling protocol as a valuable experimental approach to better understand disease progression and to screen and evaluate efficacy of novel therapeutics for DMD. Future studies can further apply cycling protocols to replicate muscle function in activities involving more strenuous eccentric contractions, such as walking down stairs or downhill [59], to better understand the impact on dystrophic muscles. Our results also indicated the need for future studies to use mouse models that more closely reflect the pathological features of DMD [77]. The cycling protocol with the ability to mimic the time-varying strain and activation patterns of human muscles in locomotion in smaller mouse muscles may also have extended use for understanding muscle mechanics in general, since it more closely replicates *in vivo* muscle function in locomotion than the traditional work loop technique [78]. Indeed, this approach has been used to demonstrate the importance of muscle force-velocity properties, activation intensity and spindle abundance on the appropriate interpretations of *in vivo* muscle functions [79–81]. Given that details of the gait cycling protocol were described in our Methods paper [17] and modified stimulator (Model 701C) is available through Aurora Scientific Inc., we expect that more studies using this or a similar approach will come out in the near future.

Supporting information

S1 Fig. The typical force responses during the eccentric contraction protocol for WT EDL muscle at 10% (A), 20% (B) and 30% (C) L_o, and for mdx EDL muscle at 10% (D), 20% (E) and 30% (F) L_o. The length changes used in the eccentric contractions at 10%, 20% and 30% Lo are shown in (G), (H) and (I), respectively. For clarity only the responses of the 1st, 3rd and 5th eccentric contractions are shown.
(DOCX)

Acknowledgement

Author contributions

Conceptualization: Xiao Hu, Allison N. McCrady, Katherine E. Bukovec, Shayn M. Peirce, Robert W. Grange, Silvia S. Blemker.

Data curation: Xiao Hu, Allison N. McCrady, Katherine E. Bukovec, Emily Y. Miller, Rachel K. Bour, Anthony C. Bruce, Katherine B. Crump, Robert W. Grange.

Formal analysis: Xiao Hu, Allison N. McCrady, Katherine E. Bukovec, Claire Yuan, Emily Y. Miller, Robert W. Grange, Silvia S. Blemker.

Funding acquisition: Shayn M. Peirce, Robert W. Grange, Silvia S. Blemker.

Investigation: Xiao Hu, Allison N. McCrady, Katherine E. Bukovec, Claire Yuan, Robert W. Grange, Silvia S. Blemker.

Methodology: Xiao Hu, Katherine E. Bukovec, Emily Y. Miller, Robert W. Grange, Silvia S. Blemker.

Project administration: Robert W. Grange.

Supervision: Shayn M. Peirce, Robert W. Grange, Silvia S. Blemker.

Writing – original draft: Xiao Hu, Allison N. McCrady.

Writing – review & editing: Xiao Hu, Allison N. McCrady, Katherine E. Bukovec, Claire Yuan, Emily Y. Miller, Rachel K. Bour, Anthony C. Bruce, Katherine B. Crump, Shayn M. Peirce, Robert W. Grange, Silvia S. Blemker.

References

1. Duan D, Goemans N, Takeda S, Mercuri E, Aartsma-Rus A. Duchenne muscular dystrophy. Nat Rev Dis Primers. 2021;7(1):13. https://doi.org/10.1038/s41572-021-00248-3 PMID: 33602943

2. Min Y-L, Bassel-Duby R, Olson EN. CRISPR Correction of Duchenne Muscular Dystrophy. Annu Rev Med. 2019;70:239–55. https://doi.org/10.1146/annurev-med-081117-010451 PMID: 30379597

3. Chemello F, Olson EN, Bassel-Duby R. CRISPR-Editing Therapy for Duchenne Muscular Dystrophy. Hum Gene Ther. 2023;34(9–10):379–87. https://doi.org/10.1089/hum.2023.053 PMID: 37060194

4. Wilton-Clark H, Yokota T. Biological and genetic therapies for the treatment of Duchenne muscular dystrophy. Expert Opin Biol Ther. 2023;23(1):49–59. https://doi.org/10.1080/14712598.2022.2150543 PMID: 36409820

5. Kornegay JN, Spurney CF, Nghiem PP, Brinkmeyer-Langford CL, Hoffman EP, Nagaraju K. Pharmacologic management of Duchenne muscular dystrophy: target identification and preclinical trials. ILAR J. 2014;55(1):119–49. https://doi.org/10.1093/ilar/ilu011 PMID: 24936034

6. Hu X, Charles JP, Akay T, Hutchinson JR, Blemker SS. Are mice good models for human neuromuscular disease? Comparing muscle excursions in walking between mice and humans. Skelet Muscle. 2017;7(1):26. https://doi.org/10.1186/s13395-017-0143-9 PMID: 29145886

7. McGreevy JW, Hakim CH, McIntosh MA, Duan D. Animal models of Duchenne muscular dystrophy: from basic mechanisms to gene therapy. Dis Model Mech. 2015;8(3):195–213. https://doi.org/10.1242/dmm.018424 PMID: 25740330

8. Grange RW, Gainer TG, Marschner KM, Talmadge RJ, Stull JT. Fast-twitch skeletal muscles of dystrophic mouse pups are resistant to injury from acute mechanical stress. Am J Physiol Cell Physiol. 2002;283(4):C1090-101. https://doi.org/10.1152/ajpcell.00450.2001 PMID: 12225973

9. Petrof BJ, Shrager JB, Stedman HH, Kelly AM, Sweeney HL. Dystrophin protects the sarcolemma from stresses developed during muscle contraction. Proc Natl Acad Sci U S A. 1993;90(8):3710–4. https://doi.org/10.1073/pnas.90.8.3710 PMID: 8475120

10. Moens P, Baatsen PH, Maréchal G. Increased susceptibility of EDL muscles from mdx mice to damage induced by contractions with stretch. J Muscle Res Cell Motil. 1993;14(4):446–51. https://doi.org/10.1007/BF00121296 PMID: 7693747

11. Radley-Crabb H, Terrill J, Shavlakadze T, Tonkin J, Arthur P, Grounds M. A single 30 min treadmill exercise session is suitable for "proof-of concept studies" in adult mdx mice: a comparison of the early consequences of two different treadmill protocols. Neuromuscul Disord. 2012;22(2):170–82. https://doi.org/10.1016/j.nmd.2011.07.008 PMID: 21835619

12. Burdi R, Rolland J-F, Fraysse B, Litvinova K, Cozzoli A, Giannuzzi V, et al. Multiple pathological events in exercised dystrophic mdx mice are targeted by pentoxifylline: outcome of a large array of in vivo and ex vivo tests. J Appl Physiol (1985). 2009;106(4):1311–24. https://doi.org/10.1152/japplphysiol.90985.2008 PMID: 19131478

13. Mathur S, Vohra RS, Germain SA, Forbes S, Bryant ND, Vandenborne K, et al. Changes in muscle T2 and tissue damage after downhill running in mdx mice. Muscle Nerve. 2011;43(6):878–86. https://doi.org/10.1002/mus.21986 PMID: 21488051

14. Arnold EM, Delp SL. Fibre operating lengths of human lower limb muscles during walking. Philos Trans R Soc Lond B Biol Sci. 2011;366(1570):1530–9. https://doi.org/10.1098/rstb.2010.0345 PMID: 21502124

15. Cappellini G, Ivanenko YP, Poppele RE, Lacquaniti F. Motor patterns in human walking and running. J Neurophysiol. 2006;95(6):3426–37. https://doi.org/10.1152/jn.00081.2006 PMID: 16554517

16. McFadyen B, Winter D. An integrated biomechanical analysis of normal stair ascent and descent. J Biomech. 1988;21(9):733–44.

17. Bukovec KE, Hu X, Borkowski M, Jeffery D, Blemker SS, Grange RW. A novel ex vivo protocol to mimic human walking gait: implications for Duchenne muscular dystrophy. Journal of Applied Physiology. 2020;129(4).

18. Rajagopal A, Dembia CL, DeMers MS, Delp DD, Hicks JL, Delp SL. Full-Body Musculoskeletal Model for Muscle-Driven Simulation of Human Gait. IEEE Trans Biomed Eng. 2016;63(10):2068–79. https://doi.org/10.1109/TBME.2016.2586891 PMID: 27392337

19. John CT, Seth A, Schwartz MH, Delp SL. Contributions of muscles to mediolateral ground reaction force over a range of walking speeds. J Biomech. 2012;45(14):2438–43. https://doi.org/10.1016/j.jbiomech.2012.06.037 PMID: 22884038

20. Hu X, Blemker SS. Musculoskeletal simulation can help explain selective muscle degeneration in Duchenne muscular dystrophy. Muscle Nerve. 2015;52(2):174–82. https://doi.org/10.1002/mus.24607 PMID: 25704785

21. Pastoret C, Sebille A. mdx mice show progressive weakness and muscle deterioration with age. J Neurol Sci. 1995;129(2):97–105. https://doi.org/10.1016/0022-510x(94)00276-t PMID: 7608742

22. Muntoni F, Mateddu A, Marchei F, Clerk A, Serra G. Muscular weakness in the mdx mouse. J Neurol Sci. 1993;120(1):71–7. https://doi.org/10.1016/0022-510x(93)90027-v PMID: 8289081

23. Dangain J, Vrbova G. Muscle development in mdx mutant mice. Muscle Nerve. 1984;7(9):700–4. https://doi.org/10.1002/mus.880070903 PMID: 6543918

24. Sperringer J, Grange R. In vitro assays to determine skeletal muscle physiologic function. Methods in Molecular Biology. 2016;1460:271–91.

25. John CT, Anderson FC, Higginson JS, Delp SL. Stabilisation of walking by intrinsic muscle properties revealed in a three-dimensional muscle-driven simulation. Comput Methods Biomech Biomed Engin. 2013;16(4):451–62. https://doi.org/10.1080/10255842.2011.627560 PMID: 22224406

26. Delp SL, Loan JP, Hoy MG, Zajac FE, Topp EL, Rosen JM. An interactive graphics-based model of the lower extremity to study orthopaedic surgical procedures. IEEE Trans Biomed Eng. 1990;37(8):757–67. https://doi.org/10.1109/10.102791 PMID: 2210784

27. Thelen DG, Anderson FC. Using computed muscle control to generate forward dynamic simulations of human walking from experimental data. J Biomech. 2006;39(6):1107–15. https://doi.org/10.1016/j.jbiomech.2005.02.010 PMID: 16023125

28. Delp SL, Anderson FC, Arnold AS, Loan P, Habib A, John CT, et al. OpenSim: open-source software to create and analyze dynamic simulations of movement. IEEE Trans Biomed Eng. 2007;54(11):1940–50. https://doi.org/10.1109/TBME.2007.901024 PMID: 18018689

29. Thelen DG. Adjustment of muscle mechanics model parameters to simulate dynamic contractions in older adults. J Biomech Eng. 2003;125(1):70–7. https://doi.org/10.1115/1.1531112 PMID: 12661198

30. Charles JP, Cappellari O, Spence AJ, Hutchinson JR, Wells DJ. Musculoskeletal Geometry, Muscle Architecture and Functional Specialisations of the Mouse Hindlimb. PLoS One. 2016;11(4):e0147669. https://doi.org/10.1371/journal.pone.0147669 PMID: 27115354

31. Schindelin J, Arganda-Carreras I, Frise E, Kaynig V, Longair M, Pietzsch T, et al. Fiji: an open-source platform for biological-image analysis. Nat Methods. 2012;9(7):676–82. https://doi.org/10.1038/nmeth.2019 PMID: 22743772

32. Zuiderveld K. Contrast Limited Adaptive Histogram Equalization. Graphics Gems. 1994:474–85. https://doi.org/10.1016/b978-0-12-336156-1.50061-6

33. Bradley D, Roth G. Adaptive Thresholding using the Integral Image. Journal of Graphics Tools. 2007;12(2):13–21. https://doi.org/10.1080/2151237x.2007.10129236

34. Otsu N. A Threshold Selection Method from Gray-Level Histograms. IEEE Trans Syst, Man, Cybern. 1979;9(1):62–6. https://doi.org/10.1109/tsmc.1979.4310076

35. Caselles V, Kimmel R, Sapiro G. Geodesic active contours. International journal of computer vision. 1997;22:61–79.

36. Meyer F. Topographic distance and watershed lines. Signal Processing. 1994;38(1):113–25. https://doi.org/10.1016/0165-1684(94)90060-4

37. Kiriaev L, Baumann CW, Lindsay A. Eccentric contraction-induced strength loss in dystrophin-deficient muscle: Preparations, protocols, and mechanisms. J Gen Physiol. 2023;155(2).

38. Yu Z, Guindani M, Grieco SF, Chen L, Holmes TC, Xu X. Beyond t test and ANOVA: applications of mixed-effects models for more rigorous statistical analysis in neuroscience research. Neuron. 2022;110(1):21–35. https://doi.org/10.1016/j.neuron.2021.10.030 PMID: 34784504

39. Holm S. A simple sequentially rejective multiple test procedure. Scandinavian journal of statistics. 1979;6(1):65–70.

40. Dixon WJ. Processing Data for Outliers. Biometrics. 1953;9(1):74. https://doi.org/10.2307/3001634

41. Askew GN, Young IS, Altringham JD. Fatigue of mouse soleus muscle, using the work loop technique. J Exp Biol. 1997;200(Pt 22):2907–12. https://doi.org/10.1242/jeb.200.22.2907 PMID: 9344980

42. Kiriaev L, Kueh S, Morley JW, Houweling PJ, Chan S, North KN, et al. Dystrophin-negative slow-twitch soleus muscles are not susceptible to eccentric contraction induced injury over the lifespan of the mdx mouse. Am J Physiol Cell Physiol. 2021;321(4):C704–20. https://doi.org/10.1152/ajpcell.00122.2021 PMID: 34432537

43. Lindsay A, Southern WM, McCourt PM, Larson AA, Hodges JS, Lowe DA, et al. Variable cytoplasmic actin expression impacts the sensitivity of different dystrophin-deficient mdx skeletal muscles to eccentric contraction. FEBS J. 2019;286(13):2562–76. https://doi.org/10.1111/febs.14831 PMID: 30942954

44. Burkholder TJ, Fingado B, Baron S, Lieber RL. Relationship between muscle fiber types and sizes and muscle architectural properties in the mouse hindlimb. J Morphol. 1994;221(2):177–90. https://doi.org/10.1002/jmor.1052210207 PMID: 7932768

45. Fiorentino NM, Blemker SS. Musculotendon variability influences tissue strains experienced by the biceps femoris long head muscle during high-speed running. J Biomech. 2014;47(13):3325–33. https://doi.org/10.1016/j.jbiomech.2014.08.010 PMID: 25189094

46. Rehorn M, Blemker S. The effects of aponeurosis geometry on strain injury susceptibility explored with a 3D muscle model. Journal of Biomechanics. 2010;43(13):2574–81.

47. Macpherson PC, Schork MA, Faulkner JA. Contraction-induced injury to single fiber segments from fast and slow muscles of rats by single stretches. American Journal of Physiology-Cell Physiology. 1996;40(5):C1438.

48. Lindsay A, Baumann CW, Rebbeck RT, Yuen SL, Southern WM, Hodges JS, et al. Mechanical factors tune the sensitivity of mdx muscle to eccentric strength loss and its protection by antioxidant and calcium modulators. Skelet Muscle. 2020;10(1):3. https://doi.org/10.1186/s13395-020-0221-2 PMID: 32007101

49. García-Castañeda M, Michelucci A, Zhao N, Malik S, Dirksen R. Postdevelopmental knockout of Orai1 improves muscle pathology in a mouse model of Duchenne muscular dystrophy. J Gen Physiol. 2022;154(9):1–12. https://doi.org/10.1085/jgp.202212345

50. Head S, Williams D, Stephenson D. Abnormalities in structure and function of limb skeletal muscle fibres of dystrophic mdx mice. Proceedings Biological Sciences. 1992;248(1322):163–9.

51. Warren GL, Hayes DA, Lowe DA, Armstrong RB. Mechanical factors in the initiation of eccentric contraction-induced injury in rat soleus muscle. J Physiol. 1993;464:457–75. https://doi.org/10.1113/jphysiol.1993.sp019645 PMID: 8229813

52. Proske U, Morgan DL. Muscle damage from eccentric exercise: mechanism, mechanical signs, adaptation and clinical applications. J Physiol. 2001;537(Pt 2):333–45. https://doi.org/10.1111/j.1469-7793.2001.00333.x PMID: 11731568

53. Manning J, O'Malley D. What has the mdx mouse model of Duchenne muscular dystrophy contributed to our understanding of this disease?. J Muscle Res Cell Motil. 2015;36(2):155–67. https://doi.org/10.1007/s10974-015-9406-4 PMID: 25669899

54. Hammers DW, Hart CC, Matheny MK, Wright LA, Armellini M, Barton ER, et al. The D2.mdx mouse as a preclinical model of the skeletal muscle pathology associated with Duchenne muscular dystrophy. Sci Rep. 2020;10(1):14070. https://doi.org/10.1038/s41598-020-70987-y PMID: 32826942

55. Goudriaan M, Van den Hauwe M, Simon-Martinez C, Huenaerts C, Molenaers G, Goemans N, et al. Gait deviations in Duchenne muscular dystrophy-Part 2. Statistical non-parametric mapping to analyze gait deviations in children with Duchenne muscular dystrophy. Gait Posture. 2018;63:159–64. https://doi.org/10.1016/j.gaitpost.2018.04.038 PMID: 29751322

56. Goudriaan M, Van den Hauwe M, Dekeerle J, Verhelst L, Molenaers G, Goemans N, et al. Gait deviations in Duchenne muscular dystrophy-Part 1. A systematic review. Gait Posture. 2018;62:247–61. https://doi.org/10.1016/j.gaitpost.2018.03.020 PMID: 29579701

57. Sutherland DH, Olshen R, Cooper L, Wyatt M, Leach J, Mubarak S, et al. The pathomechanics of gait in Duchenne muscular dystrophy. Dev Med Child Neurol. 1981;23(1):3–22. https://doi.org/10.1111/j.1469-8749.1981.tb08442.x PMID: 7202868

58. Sienko Thomas S, Buckon CE, Nicorici A, Bagley A, McDonald CM, Sussman MD. Classification of the gait patterns of boys with Duchenne muscular dystrophy and their relationship to function. J Child Neurol. 2010;25(9):1103–9. https://doi.org/10.1177/0883073810371002 PMID: 20587736

59. Hu X, Pickle NT, Grabowski AM, Silverman AK, Blemker SS. Muscle Eccentric Contractions Increase in Downhill and High-Grade Uphill Walking. Front Bioeng Biotechnol. 2020;8:573666. https://doi.org/10.3389/fbioe.2020.573666 PMID: 33178672

60. DeVita P, Helseth J, Hortobagyi T. Muscles do more positive than negative work in human locomotion. J Exp Biol. 2007;210(Pt 19):3361-73.

61. Hahn D, Han S-W, Joumaa V. The history-dependent features of muscle force production: A challenge to the cross-bridge theory and their functional implications. J Biomech. 2023;152:111579. https://doi.org/10.1016/j.jbiomech.2023.111579 PMID: 37054597

62. Seiberl W, Power GA, Herzog W, Hahn D. The stretch-shortening cycle (SSC) revisited: residual force enhancement contributes to increased performance during fast SSCs of human m. adductor pollicis. Physiol Rep. 2015;3(5):e12401. https://doi.org/10.14814/phy2.12401 PMID: 25975646

63. Lee HD, Herzog W, Leonard T. Effects of cyclic changes in muscle length on force production in in-situ cat soleus. J Biomech. 2001;34(8):979–87. https://doi.org/10.1016/s0021-9290(01)00077-x PMID: 11448689

64. Rassier DE, Herzog W, Wakeling J, Syme DA. Stretch-induced, steady-state force enhancement in single skeletal muscle fibers exceeds the isometric force at optimum fiber length. J Biomech. 2003;36(9):1309–16. https://doi.org/10.1016/s0021-9290(03)00155-6 PMID: 12893039

65. Morgan DL, Whitehead NP, Wise AK, Gregory JE, Proske U. Tension changes in the cat soleus muscle following slow stretch or shortening of the contracting muscle. J Physiol. 2000;522 Pt 3(Pt 3):503–13. https://doi.org/10.1111/j.1469-7793.2000.t01-2-00503.x PMID: 10713973

66. Vandenboom R, Gittings W, Smith IC, Grange RW, Stull JT. Myosin phosphorylation and force potentiation in skeletal muscle: evidence from animal models. J Muscle Res Cell Motil. 2013;34(5–6):317–32. https://doi.org/10.1007/s10974-013-9363-8 PMID: 24162313

67. Moore R, Houston M, Iwamoto G, Stull J. Phosphorylation of rabbit skeletal muscle myosin in situ. J Cell Physiol. 1985;125(2):301–5.

68. Ismail HM, Scapozza L, Ruegg UT, Dorchies OM. Diapocynin, a dimer of the NADPH oxidase inhibitor apocynin, reduces ROS production and prevents force loss in eccentrically contracting dystrophic muscle. PLoS One. 2014;9(10):e110708. https://doi.org/10.1371/journal.pone.0110708 PMID: 25329652

69. Dubuisson N, Versele R, Planchon C, Selvais CM, Noel L, Abou-Samra M, et al. Histological Methods to Assess Skeletal Muscle Degeneration and Regeneration in Duchenne Muscular Dystrophy. Int J Mol Sci. 2022;23(24):16080. https://doi.org/10.3390/ijms232416080 PMID: 36555721

70. Pavone AM, Giannone AG, Cabibi D, D'Aprile S, Denaro S, Salvaggio G, et al. Digital Pathology: A Comprehensive Review of Open-Source Histological Segmentation Software. BioMedInformatics. 2024;4(1):173–96. https://doi.org/10.3390/biomedinformatics4010012

71. Klemencic A, Kovacic S, Pernus F. Automated segmentation of muscle fiber images using active contour models. Cytometry. 1998;32(4):317–26. https://doi.org/10.1002/(sici)1097-0320(19980801)32:4<317::aid-cyto9>3.0.co;2-e PMID: 9701401

72. Eilbert JL, Gallistel CR, McEachron DL. The variation in user drawn outlines on digital images: effects on quantitative autoradiography. Comput Med Imaging Graph. 1990;14(5):331–9. https://doi.org/10.1016/0895-6111(90)90107-m PMID: 2224831

73. Lin MC, Ebihara S, El Dwairi Q, Hussain SN, Yang L, Gottfried SB, et al. Diaphragm sarcolemmal injury is induced by sepsis and alleviated by nitric oxide synthase inhibition. Am J Respir Crit Care Med. 1998;158(5 Pt 1):1656–63. https://doi.org/10.1164/ajrccm.158.5.9803112 PMID: 9817721

74. Ebihara S, Hussain SNA, Danialou G, Cho W-K, Gottfried SB, Petrof BJ. Mechanical ventilation protects against diaphragm injury in sepsis: interaction of oxidative and mechanical stresses. Am J Respir Crit Care Med. 2002;165(2):221–8. https://doi.org/10.1164/ajrccm.165.2.2108041 PMID: 11790659

75. Smith LR, Barton ER. SMASH - semi-automatic muscle analysis using segmentation of histology: a MATLAB application. Skelet Muscle. 2014;4:21. https://doi.org/10.1186/2044-5040-4-21 PMID: 25937889

76. Wen Y, Murach KA, Vechetti IJ Jr, Fry CS, Vickery C, Peterson CA, et al. MyoVision: software for automated high-content analysis of skeletal muscle immunohistochemistry. J Appl Physiol (1985). 2018;124(1):40–51. https://doi.org/10.1152/japplphysiol.00762.2017 PMID: 28982947

77. Yucel N, Chang AC, Day JW, Rosenthal N, Blau HM. Humanizing the mdx mouse model of DMD: the long and the short of it. NPJ Regen Med. 2018;3:4. https://doi.org/10.1038/s41536-018-0045-4 PMID: 29479480

78. Rice N, Bemis C, Daley M, Nishikawa K. Understanding muscle function during perturbed in vivo locomotion using a muscle avatar approach. Journal of Experimental Biology. 2023;226(13).

79. Charles JP, Kissane RWP, Askew GN. The impacts of muscle-specific force-velocity properties on predictions of mouse muscle function during locomotion. Front Bioeng Biotechnol. 2024;12:1436004. https://doi.org/10.3389/fbioe.2024.1436004 PMID: 39108597

80. Kissane R, Bates K, Fagan M, Wang L, Watson P, Askew G. The functional role of the rabbit digastric muscle during mastication. Journal of Experimental Biology. 2024;227(18).

81. Kissane R, Askew G. The importance of muscle activation on the interpretation of muscle mechanical performance. Journal of Experimental Biology. 2024;227(21).